

PAPER

Optical properties of chemical vapor deposition-grown PtSe₂ characterized by spectroscopic ellipsometry

To cite this article: Junfang Xie *et al* 2019 *2D Mater.* **6** 035011

View the [article online](#) for updates and enhancements.

Recent citations

- [Temperature-dependent optical and vibrational properties of PtSe₂ thin films](#)
Desman P. Gulo *et al*
- [Two-Dimensional Platinum Diselenide: Synthesis, Emerging Applications, and Future Challenges](#)
Youning Gong *et al*
- [2D Nanomaterial-Based Surface Plasmon Resonance Sensors for Biosensing Applications](#)
Sachin Singh *et al*

2D Materials



PAPER

Optical properties of chemical vapor deposition-grown PtSe₂ characterized by spectroscopic ellipsometry

RECEIVED
18 December 2018

REVISED
20 March 2019

ACCEPTED FOR PUBLICATION
29 March 2019

PUBLISHED
23 April 2019

Junfang Xie¹, Di Zhang¹, Xiao-Qing Yan¹, Mengxin Ren¹, Xin Zhao², Fang Liu¹, Ruoxuan Sun¹, Xiaokuan Li¹, Zhi Li¹, Shuqi Chen¹, Zhi-Bo Liu¹ and Jian-Guo Tian¹

¹ Key Laboratory of Weak-Light Nonlinear Photonics, Ministry of Education, School of Physics, Nankai University, Tianjin 300071, People's Republic of China

² School of Physical Science and Technology, Tianjin Polytechnic University, Tianjin 300387, People's Republic of China

E-mail: yanxq01@nankai.edu.cn and jjtian@nankai.edu.cn

Keywords: transition metal dichalcogenides, PtSe₂, optical constants, spectroscopic ellipsometry, Fourier transform infrared spectra
Supplementary material for this article is available [online](#)

Abstract

PtSe₂, an emerging 2D group-10 transition metal dichalcogenide (TMD), has aroused significant attention recently due to its intriguing physical properties. Here, the optical properties of chemical vapor deposition-grown PtSe₂ films with different thicknesses were characterized with nondestructive spectroscopic ellipsometry and Fourier transform infrared spectroscopy. The polarized optical microscopy reveals the isotropic in-plane optical response of the continuous PtSe₂ films in a scale size of at least as small as $143 \times 108 \mu\text{m}^2$. The electrical transport characterization and UV-mid infrared absorption spectra reveal the coexistence of both semiconducting and metallic contents in these PtSe₂ films, making PtSe₂ quite different among the 2D material family. The effective refractive index (n) and the extinction coefficient (k) over a spectra range of 360–1700 nm were obtained. In contrast to other TMDs, the values of n and k of PtSe₂ were found to have a strong dependence on the thickness and they decrease as the reduction of thickness. This work is conducive to provide vital parameters for further study on PtSe₂ and could facilitate its application in optoelectronic devices.

Many interesting phenomena and unique properties given by reduced dimensions make 2D materials very attractive recently [1, 2]. These 2D materials include graphene [3], black phosphorus [4] and TMDs, among which TMDs show promising application in optoelectronic and photonic devices (such as, solar cell, sensor, and photodetector) due to the tunable bandgap, high carrier mobility and large optical absorption [6–9]. For manipulating the application of these 2D materials, there has been much research on the optical and electronic properties of TMDs [10, 11]. These works mainly focused on the classic TMDs with 2H-phase, such as MoS₂ and WSe₂ *et al* [10, 11].

Platinum diselenide (PtSe₂) is a group-10 TMD with 1T-phase. Many methods are employed to synthesize PtSe₂, such as direct selenization of Pt film, thermally assisted conversion (TAC) and chemical vapor deposition (CVD) [12–14]. The strong interlayer interaction and intrinsic quantum confinement effect make the bandgap of PtSe₂ greatly tunable,

leading to a type-II Dirac semimetal-to-semiconductor transition when going from bulk to few-layer form and exhibiting a biggest bandgap of ~ 1.2 eV for monolayer (ML) PtSe₂ (from theoretical prediction) [14, 15]. Furthermore, the bandgap of PtSe₂ can be modulated by applying different types of strain [16]. Among the studied TMDs, the carrier mobility of ML PtSe₂ is the highest and comparable to that of black phosphorus [17]. In addition, the Raman spectrum [18] and absorption spectrum [19] of PtSe₂ show strong dependence on the thickness. The interesting properties render it be a top-priority candidate for functional material in transistors, photodetectors, optical sensors, chemiresistors and photocatalysts [12, 14, 15]. Manipulating the application of PtSe₂ in optoelectronic and photonic fields requires an accurate description of their optical response. Thus, it is necessary to know the optical constants (i.e. refractive index n and extinction coefficient k) of PtSe₂ and how the values vary with the thickness. Moreover, the k spectrum is a macroscopic

fingerprint of elementary excitations (such as, inter-band transition, plasmons). However, the optical constants of PtSe₂ have not yet been studied before.

To obtain the intrinsic optical properties of the materials, it is imperative to find a nondestructive measuring method. Spectroscopic ellipsometry (SE) is a sensitive (~ 0.1 Å) technique to characterize 2D materials [10, 11, 20, 21]. Ellipsometers employ light as a measurement probe, which is easy to perform and has no destructive effect on the sample. The data acquired from the SE are the amplitude ratio (ψ) and phase difference (Δ) between p- and s-polarized waves of the reflected light, which are defined by

$$\rho = \tan(\psi) \exp(i\Delta) = r_p/r_s = \left(\frac{E_{rp}}{E_{ip}}\right) / \left(\frac{E_{rs}}{E_{is}}\right) \quad (1)$$

where r_p and r_s are the reflection coefficients for the p- and s-polarized lights, respectively. With the measured ψ and Δ , the curves of wavelength-dependent optical constants (n, k) and the thickness (d) of the sample can be extracted precisely. Further, some other vital optical properties of the sample, such as absorption coefficient and bandgap can be derived [22]. SE could be used for measuring both dielectric films and metal films [23].

In this work, we present a systematic study on the optical properties of thin CVD-grown PtSe₂ films in the thickness range from about 2.0 nm up to 7.8 nm. The isotropic optical response was verified by polarized optical microscopy for these PtSe₂ continuous films. Both the electrical transport characterization and the UV-mid infrared optical absorption spectra suggest that there are both semiconducting and metallic contents in each PtSe₂ film. The optical constants in a large spectral range of 360–1700 nm were extracted from ellipsometer measurements for these PtSe₂ films.

The PtSe₂ thin films were grown by CVD technology on sapphire substrates ($\sim 1 \times 1 \times 0.03$ cm³, 6Carbon Technology, Shenzhen). The detailed growth process is presented in the supplementary material (stacks.iop.org/TDM/6/035011/mmedia). Six PtSe₂ thin films with different thicknesses, which were controlled via deposition time, were measured and labeled as samples A–F (figure 1 and table 1). As the film thickness increases, the color of the film tends to be darker (figure 1(a)). The optical microscopy image (under $10 \times$ objective) of sample B is illustrated in figure 1(b), which indicates that the film is uniform in a large scale size. The layer thickness and surface topography of the PtSe₂ samples were measured by atomic force microscopy (AFM). Figure 1(c) presents the AFM image of sample B, and the film thickness is determined to be ~ 3.3 nm. The optical microscopy and AFM images of other samples are presented in figure S1 of the supplementary material. The film thicknesses measured from AFM are listed in table 1.

Raman spectra of PtSe₂ films are illustrated in figure 1(d). Two prominent peaks can be found at ~ 177 cm⁻¹ and ~ 206 cm⁻¹, corresponding to the in-plane E_g and out-of-plane A_{1g} vibrational modes of

Se atom, respectively [17]. As the thickness increases, the intensities of both modes increase up to 6.1 nm-thickness and then decrease for 7.8 nm sample. Similar dependence of Raman intensity on film thickness had been observed in graphene, MoS₂ and WS₂ and it is primarily ascribed to the optical interference of the excitation laser and the excited Raman radiation [24–26].

To obtain their chemical state, the PtSe₂ films were monitored by x-ray photoemission spectroscopy (XPS). The Pt 4f spectrum shown in figure 1(e) can be de-convoluted into two contributions: (1) The main peaks at 73.2 eV and 76.5 eV are attributed to Pt 4f_{7/2} and Pt 4f_{5/2} associated with PtSe₂, respectively [27]; (2) Another one at 74.1 eV is attributed to Al 2p of the sapphire substrate [28]. Besides, the Se 3d peaks at 54.4 eV and 55.3 eV (figure 1(f)) reveal the characteristic signals of PtSe₂. These characteristic peaks are consistent with those in [29]. In addition, the Se:Pt stoichiometric ratios could be extracted from the XPS analysis (table 1). The results show the ratios of all the films are about 2.2, indicating the p-type doping in these films.

The absorption spectra of the PtSe₂ films were measured in the spectral range of 360–3300 nm. The spot size of incident beam was $\sim 2 \times 2$ mm², analogous to the spot size of the following SE measurements. As shown in figure 2(a), two prominent peaks can be observed in these samples except sample A. The first peak around 450 nm is without obvious shift as the thickness increases; the second peak has an obvious redshift as the thickness increases. The absorption intensity after the second peak decreases as the wavelength increasing from 800 to 2200 nm. The absorptions in the range of 2200–3300 nm are non-zero and change gently with the wavelength. As the wavelength further increases to 3300 nm, unusual slight increases are observed in the absorption spectra for all the films (figure 2(b)), indicating the possible metallic behavior in these PtSe₂ films. As anticipated, pronounced absorption enhancement for thicker film could be observed for wavelength smaller than 1800 nm. For comparison, we also measured the absorption spectrum of a 5.1 nm-thick Au film (see figure S2 in the supplementary material), which is close to the percolation threshold at about 5 nm. As shown in the inset of figure 2(a), there is obvious optical absorption in the infrared region in the Au-film, but the optical absorption of Au-film does not prominently increase with the wavelength and could not be described by the Drude model, which is due to the fact that the thickness of Au film is close to the percolation threshold [30]. The wavelength dependence of the infrared optical absorption is nearly similar in these PtSe₂ and Au films, suggesting the possible metallic content in each PtSe₂ film. It is noted that the measurements at different positions did not give rise to visible variation in these absorption spectra, confirming the good uniformity of these films.

Further analysis of the phases from the absorption spectra is limited by the maximum detectable wavelength of the spectrophotometer. In order to

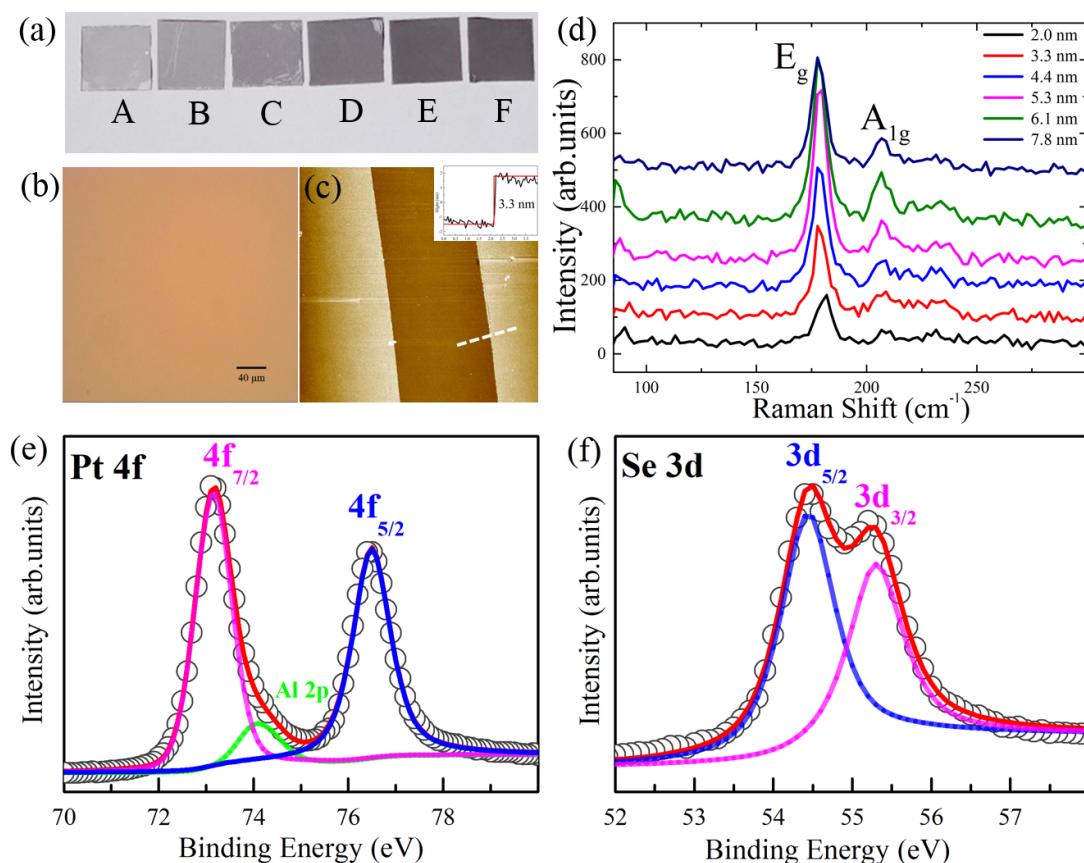


Figure 1. (a) Photographs of PtSe₂ samples with increasing thickness. (b) Optical microscopy image with a bar of 40 μm and (c) AFM image of sample B, the inset shows the thickness of ~ 3.3 nm. (d) Raman spectra with an excitation wavelength of 514 nm. (e) and (f) XPS spectra of Pt 4f and Se 3d regions of PtSe₂. The black circle is the experimental data, the lines are the processed single peak, the red curves are the results of XPS peak analysis.

Table 1. Growth time of the samples and the corresponding thickness determined by AFM and SE, as well as the Se:Pt stoichiometric ratios.

	Growth time	Thickness (by AFM)	Thickness (by SE)	$n_{\text{Se}}/n_{\text{Pt}}$
Sample A	5 min	2.0 nm	2.0 nm	2.23
Sample B	7 min	3.3 nm	3.6 nm	2.15
Sample C	10 min	4.4 nm	4.5 nm	2.17
Sample D	12 min	5.3 nm	5.6 nm	2.14
Sample E	15 min	6.1 nm	6.0 nm	2.11
Sample F	20 min	7.8 nm	8.0 nm	2.19

ascertain the phases and electronic behavior in these PtSe₂ films, electrical transport characterizations were performed on the transistors implemented in our samples. Figure 3 shows the drain current I_{DS} as a function of the applied gate voltage V_g . The conductance could be varied by the gate voltage. With decreasing the thickness, stronger gate modulation could be obtained. All results suggest that the devices show a p-type doped semiconductor behavior with an obvious current modulation by the gate voltage, indicating that there is a semiconducting phase in these multilayer PtSe₂ films. It is noted that these results are consistent with the Se:Pt stoichiometric ratios extracted from XPS.

To ascertain whether there is optical anisotropy in the 2D surface of these CVD grown PtSe₂ films which are expected to have randomly oriented grains, we took two kinds of optical measurements. The first method is polarized optical microscopy imaging. The detailed diagram of setup is shown in figure S3 of the supplementary material. The analyzed area was about $143 \times 108 \mu\text{m}^2$, smaller than the counterpart of SE. A CCD camera was used to capture the angle-dependent optical images. We extracted the intensity of three channels of red, green, blue (RGB) and the total intensity ($0.299R + 0.587G + 0.114B$) at different rotation angles [31]. It could be seen from figure 4(a) that the optical intensity has no obvious change with the rotation angle. In figure 4(b), the reflected light intensities of RGB channels and the total intensity maintain almost invariable with the rotation angle, which indicates the optical isotropy of the PtSe₂ films [5, 32]. Results of other samples are shown in figure S4 of the supplementary material. Therefore, we conclude that the in-plane optical response of the PtSe₂ film is isotropic for analyzed area as small as $143 \times 108 \mu\text{m}^2$. Another method we adopted is polarization-dependent optical absorption measurement, which suggests the in-plane isotropic optical absorption in PtSe₂ films (figure S5 of the supplementary material). In addition, the transmissions of focused femtosecond pulses

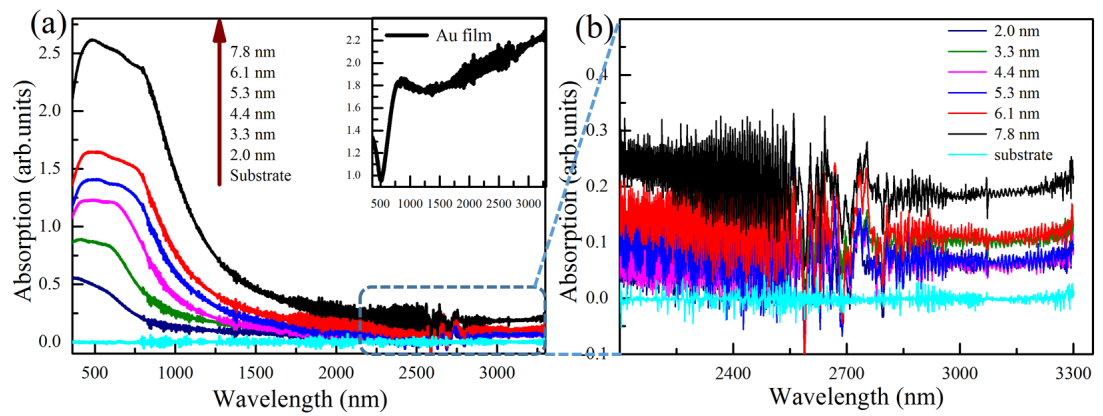


Figure 2. (a) Absorption spectra of samples A–F and the sapphire substrate. The inset shows the absorption spectrum of the 5.1 nm-thick Au film fabricated by magnetron sputtering. (b) The enlargement of (a). The oscillations in these curves in the infrared region are from the interference effects caused by the substrate.

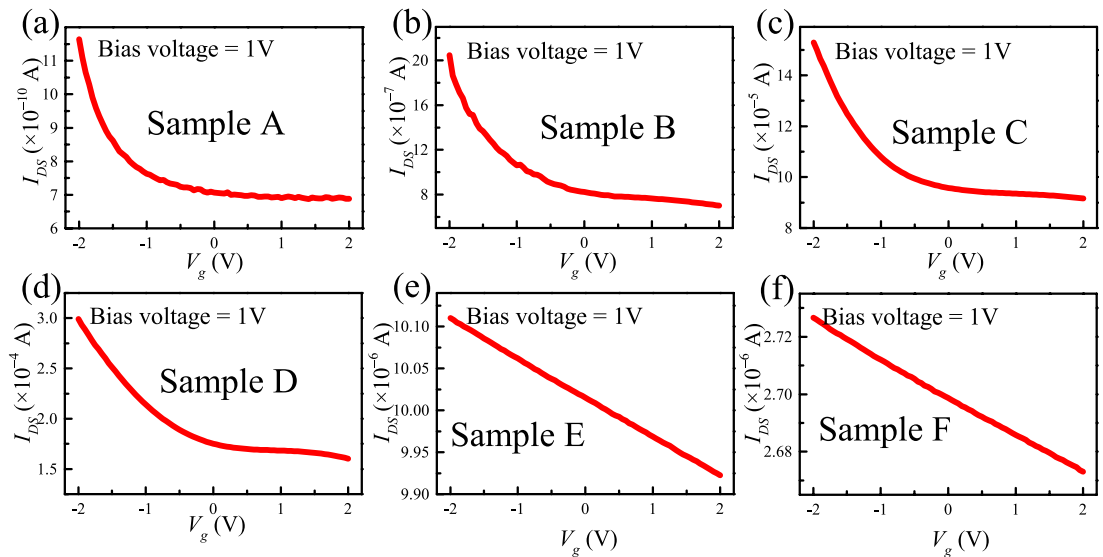


Figure 3. (a)–(f) I_D – V_g curves recorded for samples A–F respectively, showing p-type semiconducting behavior.

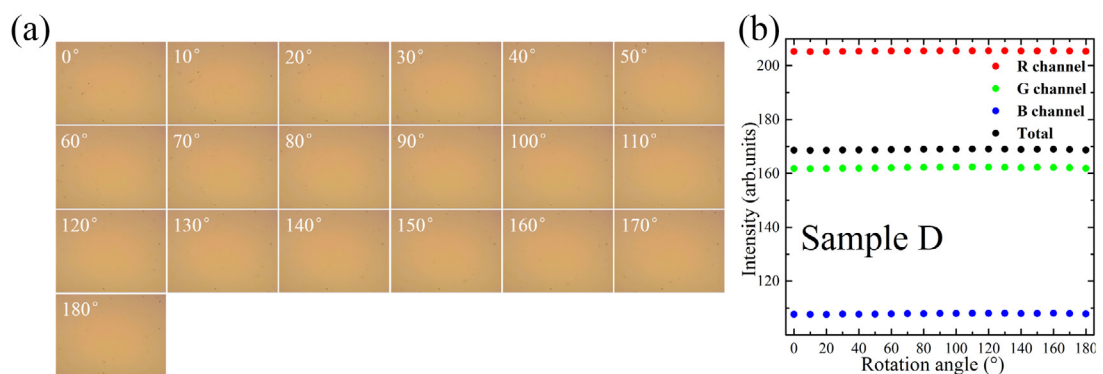


Figure 4. (a) Optical microscopic images of sample D at different rotation angles. (b) The intensities of RGB channels and the total intensity as a function of rotation angle.

(beam waist radius of $\sim 33 \mu\text{m}$ for 800 nm, and $\sim 14 \mu\text{m}$ for 400 nm) are polarization independent (not shown here). The isotropic optical response of PtSe_2 film is attributed to that the CVD-grown 2D materials

are polycrystalline [27], and the size of single crystal domain is much smaller than the analyzed area used in our measurements. For polycrystalline materials and for the materials where the stoichiometry

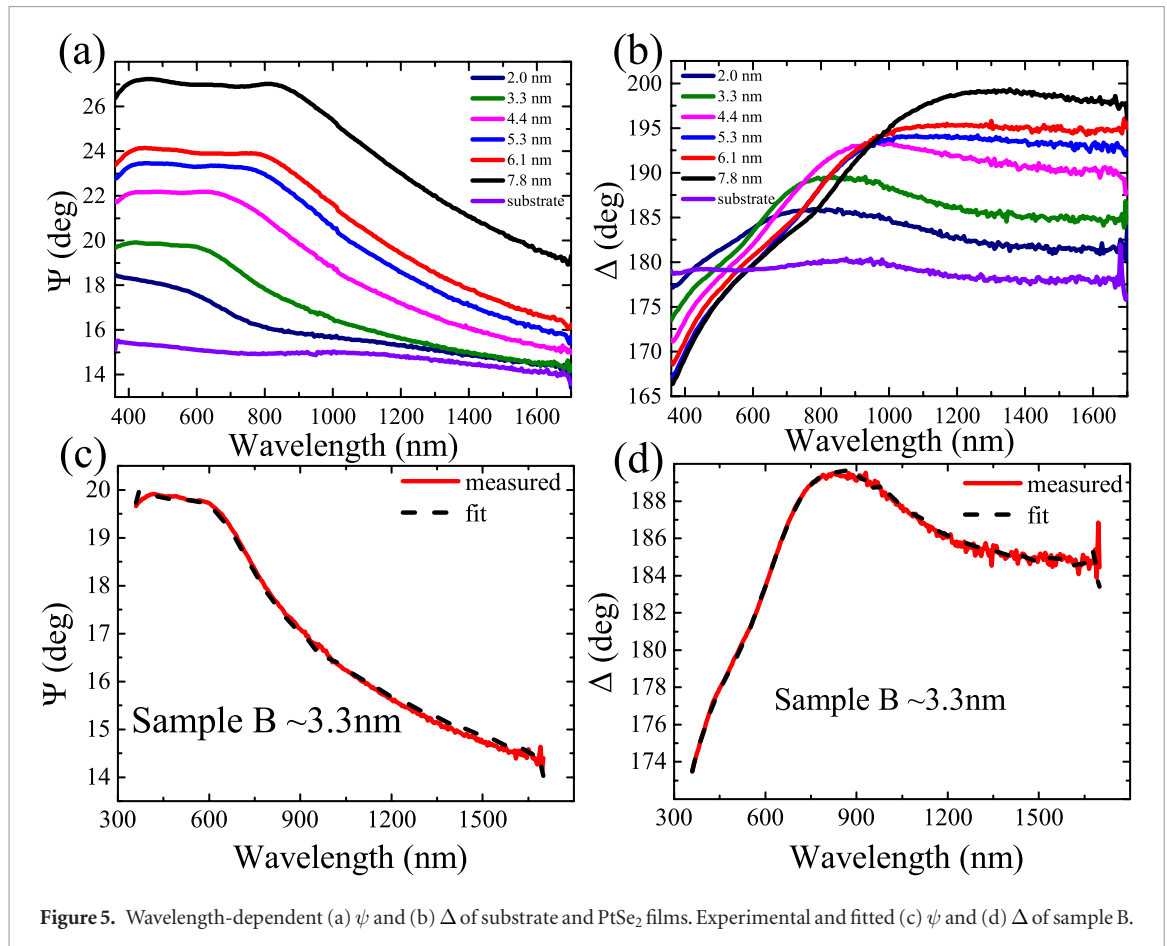


Figure 5. Wavelength-dependent (a) ψ and (b) Δ of substrate and PtSe₂ films. Experimental and fitted (c) ψ and (d) Δ of sample B.

or bandgap/structure may vary with the process of growth (such as growth time), the optical constants may be different from their crystal forms and should be specifically determined [23]. Thus, it is inferred that the optical constants of these PtSe₂ films would be different and the determination of the optical constants for each film is of importance.

To determine the effective optical constants of the PtSe₂ films, the SE measurements were performed by using an ellipsometer (Accurion EP4) over a spectra range from 360 nm to 1700 nm with a step size of 5 nm and at an incidence angle of 50°. The analyzed area of our ellipsometer was $200 \times 200 \mu\text{m}^2$. The experimental setup was similar to the imaging ellipsometer setup used by Wurstbauer *et al* [33, 34]. The detailed SE measurements of the PtSe₂ films are shown in the supplementary material. In the SE measurements, we concerned the polarization state changes of reflected light, and the ellipsometric parameters Δ and ψ can be extracted directly from SE. Four-zone measurement method was applied to minimize measurement errors [33]. The reflected light from the back surface of the sapphire substrate was shielded by a blade, and the influence of the scattered light was so little that it could be ignored. The optical constants of the sapphire substrate were measured by SE in the same condition. In the experimental configuration, only the in-plane optical properties and parameters were probed since the out-of-plane optical response was hindered by the extremely short path length of the light through these PtSe₂ thin films [36].

We can derive the optical constants and thicknesses of the PtSe₂ films by analyzing the phase and amplitude changes of the reflected light from the sample surface. The measured ψ and Δ of the PtSe₂ films are depicted in figure 5. Clearly, ψ and Δ spectra of the PtSe₂ films show a strong dependence on the film thickness. With the precisely measured ψ and Δ , we developed an optical model consisting of sapphire substrate/PtSe₂ film/air ambient structure and applied the Fresnel equations to extract the optical constants of the PtSe₂ films. The thickness of sapphire substrate could be considered to be infinite, and the PtSe₂ thickness was assumed to be unknown. The spectra of ψ and Δ were fitted by the appendant data processing software of the ellipsometer, further obtaining the spectra of n and k from fitting. To evaluate the goodness of fit, the root mean square error (RMSE) is defined by

$$\text{RMSE} = \sqrt{\frac{1}{N - P + 1} \chi^2}. \quad (2)$$

The RMSE should be close to one for an ideal fit. A superimposed line shape (Lorentz + Tauc-Lorentz (T-L) + eps) was used in the fits to extract the n and k , therein Lorentz and T-L oscillators described the shape of the curves whereas eps was used to shift the curves up and down. Another superimposed line shape (Lorentz + Tauc-Lorentz (T-L) + Drude + eps) had been tried. However, the extracted results had no obvious change but fairly big error emerged (see tables S2, S3 and figure S7 of the supplementary

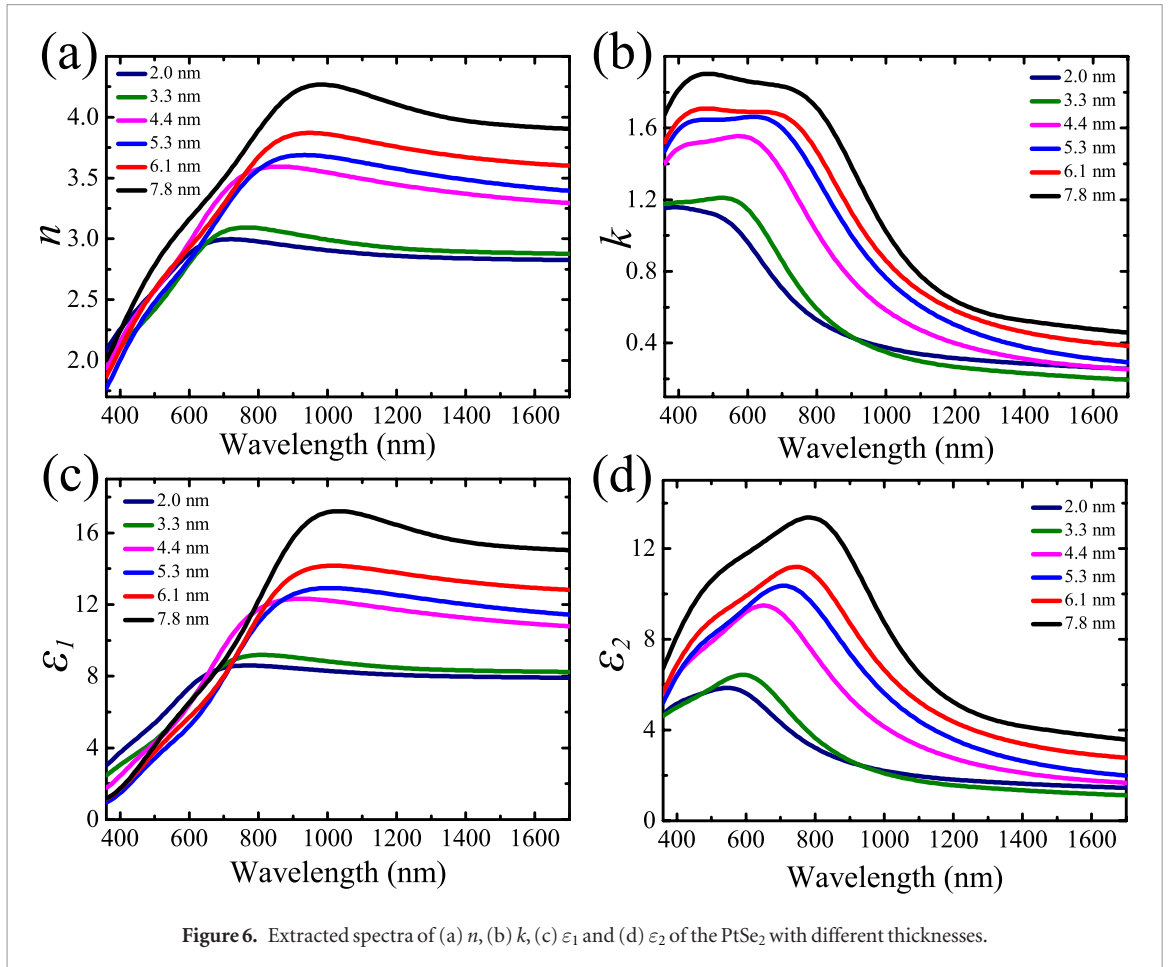


Figure 6. Extracted spectra of (a) n , (b) k , (c) ε_1 and (d) ε_2 of the PtSe₂ with different thicknesses.

material). The parameters were obtained from fitting when the RMSE was minimum. The comparisons of ψ and Δ between experiment and fit are depicted in figures 5(c) and (d) for sample B, showing good agreement between experiment and fitting. Moreover, the real and imaginary parts of the complex dielectric function ($\varepsilon = \varepsilon_1 + i\varepsilon_2$) can be extracted from the fits. The results of other samples are presented in figure S6 of the supplementary material, and more information about the fits can be found there.

The film thicknesses extracted from SE fits are in good agreement with those determined by AFM (table 1). Figure 6 illustrates the dependence of the extracted n , k , ε_1 and ε_2 on the wavelength for PtSe₂ films. We find a strong correlation between the value of n and the thickness. That is, the thicker the sample is, the larger the n value is, which is more obvious in the long wavelength region. In addition, with the increase of wavelength, the n value first increases sharply and then decreases slowly to a certain value. The peak shows a distinct redshift as the thickness increases. There are two dominant peaks in the k spectra of these films except A (figure 6(b)), and they get closer as the thickness decreases. In all cases, as the wavelength increases, the value of k has no obvious change in the short wavelength region and decreases sharply in the region of 600–1200 nm, and then approaches to a constant value. Furthermore, the value of k increases with the thickness. In figures 6(c) and (d), there is an almost

identical trend between ε_1 and n . A distinct peak can be found in the ε_2 plot and it shows obvious redshift for thicker films. By comparing the results in figures 2(a) and 6(b), we found that the trends of k are almost similar to the absorption spectra, thus, providing complementary validation for the values. The reserved extinction coefficient for wavelength larger than 1400 nm could not be from the excess Se component, since the k value of Selenium is zero for wavelength larger than 800 nm [35]. So, the large k value should merely origin from the PtSe₂.

Furthermore, we calculated the nominal optical bandgap on the basis of the absorption coefficient α from absorption spectra (figure 2). The photon energy is related to absorption coefficient α by

$$\alpha = \frac{K(h\nu - E_g)^m}{h\nu} \quad (3)$$

where K is a constant, $h\nu$ is the incident photon energy, m is a number that characterizes the bandgap transition process. m gets a value of 1/2 for direct transition and 2 for indirect transition [10, 11]. Since PtSe₂ is considered to be indirect bandgap material [15, 37], we have $m = 2$. Equation (3) can be expressed as

$$K^{-1/2}(\alpha h\nu)^{1/2} = h\nu - E_g. \quad (4)$$

As indicated in equation (4), when $(\alpha h\nu)^{1/2} = 0$, we have $h\nu = E_g$. So, the optical bandgap can be extracted

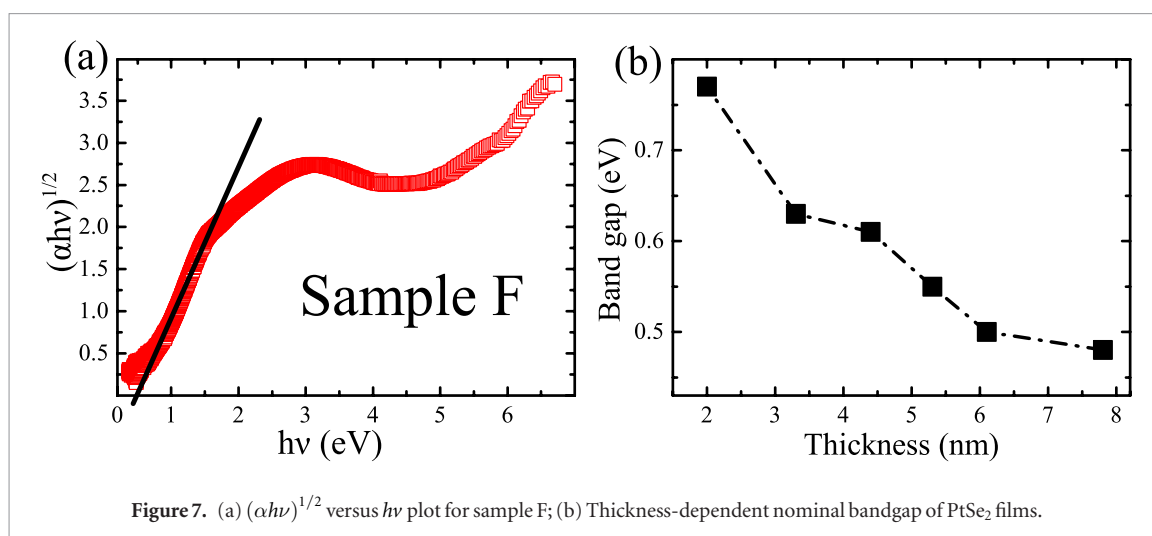


Figure 7. (a) $(\alpha h\nu)^{1/2}$ versus $h\nu$ plot for sample F; (b) Thickness-dependent nominal bandgap of PtSe₂ films.

by extending the tangent line of the linearity region of a $(\alpha h\nu)^{1/2}$ versus $h\nu$ plot to $(\alpha h\nu)^{1/2} = 0$, then the abscissa of the intersection point can be considered as the magnitude of the bandgap. $(\alpha h\nu)^{1/2}$ versus $h\nu$ plot of sample F is displayed in figure 7(a), indicating that the nominal bandgap of 7.8 nm-thick PtSe₂ is ~ 0.48 eV. Additional $(\alpha h\nu)^{1/2}$ versus $h\nu$ plots for other samples are presented in figure S8 of the supplementary material. The thickness-dependent bandgap of our PtSe₂ films is shown in figure 7(b). The obtained nominal optical bandgap locates in the range from 1614 nm to 2590 nm (i.e. 0.77–0.48 eV). However, for each PtSe₂ film, we could observe weak optical absorption for light with photon energy much smaller than the bandgap. It means that the extracted bandgaps are invalid and these PtSe₂ films are not pure semiconductor, i.e. metallic PtSe₂ contents should exist in these PtSe₂ films. In addition, we have tried to fit another linearity region of the $(\alpha h\nu)^{1/2}$ versus $h\nu$ plot and the extracted bandgaps are negative, which are not valuable for semiconductor and further support the metallic content in each PtSe₂ film (see figure S9 of the supplementary material).

To further confirm the non-pure semiconducting behavior, Fourier transform infrared spectrometer (FTIR)-based infrared spectroscopy is applied to obtain the absorption spectra in the near- and mid-infrared regions. The infrared spectroscopy was performed using a Bruker FTIR spectrometer (Vertex 70) integrated with a Hyperion 2000 microscope. Figure 8 denotes the relative optical absorption spectra of $1 - T/T_0$, where T and T_0 are the optical transmission through the PtSe₂ films on sapphire substrate and the sapphire substrate only, respectively. Clearly, weak infrared absorption could be still observed in these PtSe₂ films at even as small as 0.24 eV (5.2 μ m), and no optical resonances exist in the absorption spectra of these PtSe₂ films. The observed unexpected weak infrared absorption features further confirm that these PtSe₂ films are not pure semiconductor. As shown in figures 2 and 8, the infrared absorption of PtSe₂ films

is quite similar to that of Au films with thickness close to percolation threshold, where the Drude behavior was deviated for the metallic Au film. Based on former results from electrical transport and infrared spectra, it is concluded that there are both semiconducting and metallic contents in these PtSe₂ films, the weak infrared absorption origins from the metallic content. Owing to the extremely small thickness for the metallic contents in these PtSe₂ films, we could not observe the increase of infrared absorption as the wavelength increasing [30]. In addition, each PtSe₂ film exhibits a thickness-dependent infrared spectrum, which indicates that the metallic content increases with the thickness of PtSe₂ film. So, the measured optical constants are the results of the interplay between semiconducting and metallic contents in these PtSe₂ films. The large k in infrared region is mainly dominated by the metallic content in the film.

Based on above results, we could not judge how the semiconducting content and metallic content compose one PtSe₂ film. Former reports on epitaxial graphene show that the interaction between graphene and the substrate could alter the properties of graphene [38]. So, the observed mixed phase in PtSe₂ would be a result of the interaction between the substrate and the PtSe₂ layer via the strong coupling which results in the structure change for the PtSe₂ layer close to substrate. Other experiments should be designed to demonstrate the feature of each content in a PtSe₂ film, such as angle-resolved photoemission spectroscopy.

As shown above, there is a strong dependence of both n and k on the PtSe₂ thickness in a large range (at least, 2–7.8 nm), which is not obvious in other TMDs (such as MoS₂ and WSe₂). Eichfeld *et al* shows that the optical constants of their metalorganic CVD grown WSe₂ films do not have obvious dependence on the thickness ranging from 2 nm to 23 nm [10, 11]. The observed increase of n and k as the film thickness increases may be due to the enhancement of the interlayer interaction (i.e. van der Waals force) with PtSe₂ thickness. The two peaks in ψ spectra are corresponded to the peaks in the k spectra and absorption

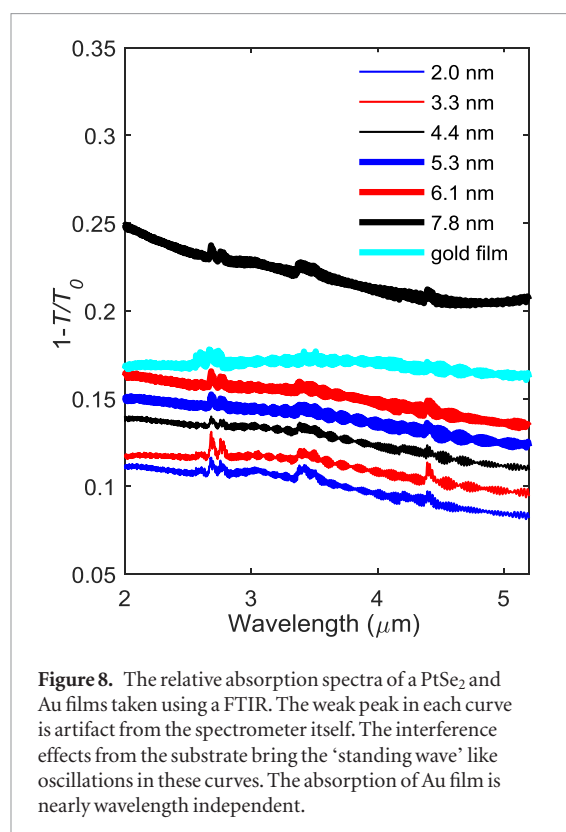


Figure 8. The relative absorption spectra of a PtSe₂ and Au films taken using a FTIR. The weak peak in each curve is artifact from the spectrometer itself. The interference effects from the substrate bring the ‘standing wave’ like oscillations in these curves. The absorption of Au film is nearly wavelength independent.

spectra. The strong dependence of both n and k on the thickness greatly facilitates PtSe₂ toward functional optoelectronic materials since the thickness supplies another degree of freedom for us to modulate optical constants and further to design optoelectronic devices. It’s worth mentioning that the variation tendencies of n and k with wavelength are similar to those of graphene [39, 40]. This study filled the gaps in knowledge of the optical properties of 1T-phase TMDs, expediting the application of PtSe₂ in optoelectronic devices.


In summary, the optical properties of CVD-grown continuous p-type doped PtSe₂ films with thickness range from 2.0 nm to 7.8 nm were measured by non-destructive SE, Fourier transform infrared spectroscopy and polarized optical microscopy. The PtSe₂ films exhibit an in-plane optical isotropic response. These PtSe₂ films have a mixed phase: both semiconducting and metallic contents coexist in each film. As a result, near wavelength-independent weak infrared absorption could be observed in these PtSe₂ films due to the presence of extremely thin metallic content in the film. The values of effective n and k extracted from SE increase as the film thickness increasing. The tunable optical constants are conducive to provide vital parameters for precise optical analysis and analog simulation, promoting future developments and applications of PtSe₂.

Acknowledgments

We thank Haowei Guo for transferring the PtSe₂ films onto the silicon. This work was supported by the

National Key Scientific Instrument and Equipment Development Project of China (2013YQ030595); the National Natural Science Foundation of China (Nos. 11504265, 11304166, 61775106, 11711530205); and the National Key Research and Development Program of China (Nos. 2016YFA0301102, 2017YFA0305100).

ORCIDiDs

Xiao-Qing Yan  <https://orcid.org/0000-0001-5823-1328>

References

- [1] Periyannagounder D, Gnanasekar P, Varadhan P, He J-H and Kulandaivel J 2018 *J. Mater. Chem. C* **6** 9545–51
- [2] Liu B, Long M, Cai M-Q and Yang J 2018 *J. Phys. Chem. Lett.* **9** 4822–7
- [3] Soavi G et al 2018 *Nat. Nanotechnol.* **13** 583–8
- [4] Kuriakose S, Ahmed T, Balendhran S, Collis G E, Bansal V, Aharonovich I, Sriram S, Bhaskaran M and Walia S 2018 *Appl. Mater. Today* **12** 244–9
- [5] Mao N et al 2016 *J. Am. Chem. Soc.* **138** 300–5
- [6] Li B L, Wang J, Zou H L, Garaj S, Lim C T, Xie J, Li N B and Leong D T 2016 *Adv. Funct. Mater.* **26** 7034–56
- [7] Tsai M-L, Su S-H, Chang J-K, Tsai D-S, Chen C-H, Wu C-I, Li L-J, Chen L-J and He J-H 2014 *ACS Nano* **8** 8317–22
- [8] Voiry D, Yang J and Chhowalla M 2016 *Adv. Mater.* **28** 6197–206
- [9] Mak K F and Shan J 2016 *Nat. Photon.* **10** 216
- [10] Yim C, O’Brien M, McEvoy N, Winters S, Mirza I, Lunney J G and Duesberg G S 2014 *Appl. Phys. Lett.* **104** 103114
- [11] Eichfeld S M, Eichfeld C M, Lin Y-C, Hossain L and Robinson J A 2014 *APL Mater.* **2** 092508
- [12] Yim C et al 2016 *ACS Nano* **10** 9550–8
- [13] Wang Z, Li Q, Besenbacher F and Dong M 2016 *Adv. Mater.* **28** 10224–9
- [14] Wang Y et al 2015 *Nano Lett.* **15** 4013–8
- [15] Zhuang H L and Hennig R G 2013 *J. Phys. Chem. C* **117** 20440–5
- [16] Li P, Li L and Zeng X C 2016 *J. Mater. Chem. C* **4** 3106–12
- [17] Yim C, McEvoy N, Riazimehr S, Schneider D S, Gity F, Monaghan S, Hurley P K, Lemme M C and Duesberg G S 2018 *Nano Lett.* **18** 1794–800
- [18] Maria O B et al 2016 *2D Mater.* **3** 021004
- [19] Zhao Y et al 2016 *Adv. Mater.* **29** 1604230
- [20] Liberman V, Diest K, Stull C W, Cook M T, Lennon D M, Rothschild M and Schoeche S 2016 *ACS Photonics* **3** 796–805
- [21] Liu H-L, Shen C-C, Su S-H, Hsu C-L, Li M-Y and Li L-J 2014 *Appl. Phys. Lett.* **105** 201905
- [22] Fujiwara H 2007 *Spectroscopic Ellipsometry: Principles and Applications* (New York: Wiley) (<https://doi.org/10.1002/9780470060193>)
- [23] Tompkins H G, Tasic S, Baker J and Convey D 2000 *Surf. Interface Anal.* **29** 179–87
- [24] Lee C, Yan H, Brus L E, Heinz T F, Hone J and Ryu S 2010 *ACS Nano* **4** 2695–700
- [25] Berkdemir A 2013 *Sci. Rep.* **3** 1755
- [26] Wang Y Y, Ni Z H, Shen Z X, Wang H M and Wu Y H 2008 *Appl. Phys. Lett.* **92** 043121
- [27] Zeng L-H et al 2018 *Adv. Funct. Mater.* **28** 1705970
- [28] Seal S, Krezoski S, Barr T L, Petering D H, Klinowski J and Evans P H 1996 *Proc. R. Soc. B* **263** 943–51
- [29] Yu X et al 2018 *Nat. Commun.* **9** 1545
- [30] Gompf B, Beister J, Brandt T, Pflaum J and Dressel M 2007 *Opt. Lett.* **32** 1578–80
- [31] Yao H and Gao W 2001 *Pattern Recognit.* **34** 1555–64
- [32] Xin W et al 2017 *Adv. Mater.* **30** 1704653

- [33] Matkovic A, Beltaos A, Milicevic M, Ralevic U, Vasic B, Jovanovic D and Gajic R 2012 *J. Appl. Phys.* **112** 123523
- [34] Wurstbauer U, Röling C, Wurstbauer U, Wegscheider W, Vaupel M, Thiesen P H and Weiss D 2010 *Appl. Phys. Lett.* **97** 231901
- [35] Ciesielski A, Skowronski L, Pacuski W and Szoplik T 2018 *Mat. Sci. Semicon. Proc.* **81** 64–7
- [36] Nelson F J, Kamineni V K, Zhang T, Comfort E S, Lee J U and Diebold A C 2010 *Appl. Phys. Lett.* **97** 253110
- [37] Guo G Y and Liang W Y 1986 *J. Phys. C: Solid State Phys.* **19** 995
- [38] Zhou S Y, Gweon G H, Fedorov A V, First P N, de Heer W A, Lee D H, Guinea F, Castro Neto A H and Lanzara A 2007 *Nat. Mater.* **6** 770
- [39] Li W, Cheng G, Liang Y, Tian B, Liang X, Peng L, Hight Walker A R, Gundlach D J and Nguyen N V 2016 *Carbon* **99** 348–53
- [40] Matkovic A, Ralevic U, Isic G, Jakovljevic M M, Vasic B, Milošević I, Markovic D and Gajic R 2012 *Phys. Scr.* **2012** 014069